Clim. Past Discuss., 8, 2893–2920, 2012
www.clim-past-discuss.net/8/2893/2012/
doi:10.5194/cpd-8-2893-2012

Climate of the Past Discussions

Stalagmite water content as a proxy for drip water supply in tropical and subtropical areas

N. Vogel[1,2], Y. Scheidegger[1,2], M. S. Brennwald[1], D. Fleitmann[3,4,*], S. Figura[1,5], R. Wieler[2], and R. Kipfer[1,2,5]

[1]Eawag, Swiss Federal Institute of Aquatic Science and Technology, Überlandstrasse 133, 8600 Dübendorf, Switzerland
[2]ETH Zurich, Institute of Geochemistry and Petrology, Clausiusstrasse 25, 8092 Zurich, Switzerland
[3]Institute of Geological Sciences, University of Berne, Baltzerstrasse 1–3, 3012 Berne, Switzerland
[4]Oeschger Center for Climate Research, University of Berne, Zähringerstrasse 25, 3012 Berne, Switzerland
[5]ETH Zurich, Institute of Biogeochemistry and Pollutant Dynamics, Universitätsstrasse 16, 8092 Zurich, Switzerland
[*]now at: Department of Archaeology, School of Human and Environmental Sciences, University of Reading, Whiteknights Box 226, Reading RG6 6AB, UK

Received: 15 June 2012 – Accepted: 18 June 2012 – Published: 25 July 2012

Correspondence to: N. Vogel (nadia.vogel@eawag.ch), Y. Scheidegger (yvonne.scheidegger@fastmail.fm), M. S. Brennwald (matthias.brennwald@eawag.ch), D. Fleitmann (fleitmann@geo.unibe.ch), S. Figura (simon.figura@eawag.ch), R. Wieler (wieler@erdw.ethz.ch), R. Kipfer (kipfer@eawag.ch)

Published by Copernicus Publications on behalf of the European Geosciences Union.

Abstract

In this pilot study water was extracted from samples of two Holocene stalagmites from Socotra Island, Yemen, and one Eemian stalagmite from southern continental Yemen. The amount of water extracted per unit mass of stalagmite rock, termed "water yield" hereafter, serves as a measure for its total water content. The stalagmites' water yield records vary systematically with the corresponding oxygen isotopic compositions of the calcite ($\delta^{18}O_{calcite}$). Low $\delta^{18}O_{calcite}$ values are thereby accompanied by low water yields and vice versa. Based on the paleoclimatic interpretation of the $\delta^{18}O_{calcite}$ records, water yields can be linked to drip water supply. High drip water supply caused by high precipitation rates supports homogeneous deposition of calcite with low porosity and therefore a small fraction of water-filled inclusions, resulting in low water yields of the respective samples. A reduction of drip water supply fosters irregular growth of calcite with higher porosity, leading to an increase of the fraction of water-filled inclusions and thus higher water yields. The results are consistent with the literature on stalagmite growth and supported by optical inspection of thin sections of our samples. We propose that for a stalagmite from a tropical or subtropical area, its water yield record represents a novel paleoclimate proxy recording changes in drip water supply, which can in turn be interpreted in terms of associated precipitation rates.

1 Introduction

Stalagmites have been recognised as distinguished paleoclimate archives as they occur widespread in continental settings, are precisely dateable, and preserve a wealth of high-resolution paleoclimate information over long time intervals (e.g. Cheng et al., 2009; Dong et al., 2010; Fleitmann et al., 2003a, 2007; Henderson, 2006; Wang et al., 2008; Zhao et al., 2010). For paleoclimate reconstructions, stalagmite studies often focus on changes in the isotopic compositions of oxygen and carbon of the calcite ($\delta^{18}O_{calcite}$, $\delta^{13}C_{calcite}$) to identify major climatic events (e.g. Burns et al., 2001;

CPD
8, 2893–2920, 2012

Fleitmann et al., 2009; Liu et al., 2010), to reconstruct changes in precipitation (e.g. Griffith et al., 2010; Vaks et al., 2010), and to infer type and density of plant cover above a cave (e.g. Cosford et al., 2009; Dorale et al., 1998). However, our understanding of the true sensitivity of $\delta^{18}O_{calcite}$ and $\delta^{13}C_{calcite}$ values to climatic and environmental variables remains limited and interpretation of speleothem stable isotope records is therefore often controversial (e.g. Clemens et al., 2010; LeGrande and Schmidt, 2009; McDermott et al., 2006). A way to reduce these uncertainties is to measure additional climate-sensitive parameters in speleothems. Further information on paleoclimatic conditions can for example be obtained from drip water trapped in fluid inclusions during stalagmite growth. Its hydrogen isotopic composition (in combination with corresponding $\delta^{18}O_{calcite}$) has been used to reconstruct paleotemperatures (e.g. Zhang et al., 2008) and changes in the source and amount of precipitation (e.g. Fleitmann et al., 2003b; Harmon et al., 1979; McGarry et al., 2004; Schwarcz and Harmon, 1976). More recently, concentrations of noble gases dissolved in the fluid inclusion water have been used to determine absolute temperatures prevailing in a cave during stalagmite growth (Kluge et al., 2008; Scheidegger et al., 2010, 2011). These so-called noble gas temperature determinations require the quantification of the amount of water from which the dissolved noble gases are released. In the course of noble gas temperature determinations on samples from two Holocene stalagmites from Socotra Island (Yemen), we observed that the amounts of water extracted per unit mass of stalagmite rock (the "water yields") vary systematically with the respective stalagmites' $\delta^{18}O_{calcite}$, which had previously been shown to reflect changes in the rates of precipitation (Fleitmann et al., 2007). The same co-variation of water yield and $\delta^{18}O_{calcite}$ was observed in a stalagmite grown during the Eemian in Southern Continental Yemen. Also for this stalagmite, the $\delta^{18}O_{calcite}$ record was found to reflect mainly changes in precipitation rates (Fleitmann et al., 2011). We therefore propose that a stalagmite's water yield represents a new paleoclimate proxy responding to changes in drip water supply.

CPD
8, 2893–2920, 2012

2 Experimental

2.1 Sampling sites

Figure 1 shows the locations of the caves from where the three studied stalagmites originate. Stalagmites D1 and P3 were taken from Dimarshim Cave and Pit Cave, respectively, located on opposite sides of the central mountain range of Socotra Island, Yemen. Socotra lies in the NW Indian Ocean, about 240 km east of the Horn of Africa and 380 km south of the Arabian Peninsula. The modern climatic conditions on the island are semi-arid and characterized by seasonally reversing monsoon winds (Scholte and De Geest, 2010). Rainfall is associated with the passing of the Intertropical Convergence Zone over the island, resulting in a mean annual precipitation of approximately 300 mm (Fleitmann et al., 2007; Scholte and De Geest, 2010; Shakun et al., 2007). Stalagmite Y99 was taken from Mukalla Cave (see, Fleitmann et al., 2011) situated in Southern Continental Yemen, an area that is also influenced by the monsoon. However, present-day precipitation in the Mukalla Cave region is considerably lower than on Socotra Island and is characterized by arid to hyper-arid climatic conditions.

2.2 Dating

Absolute ages for all studied stalagmites are based on Uranium-series dating (^{230}Th-dating hereafter). Details on the analytical method and results are provided by Fleitmann et al. (2007, 2011). Age models for D1 and Y99 were constructed by linear interpolation between measured ^{230}Th ages. A total of eight ^{230}Th ages (see Fig. 2) indicate that stalagmite D1 grew continuously with a mean growth rate of 0.25 mm a^{-1} over the last 4.5 ka. Stalagmite Y99 records several growth periods separated by hiatuses (Fleitmann et al., 2011). For this study the growth period between 119 and 131 ka BP was analyzed. During this period Y99 grew at a mean growth rate of about 0.013 mm a^{-1} as deduced from a total of seven ^{230}Th ages. The studied part of the stalagmite is separated from older parts by a distinct change in calcite texture and colour.

CPD
8, 2893–2920, 2012

Photographs of stalagmite Y99 including locations for dating can be found in Fig. 2 in Fleitmann et al. (2011). In this figure, the part of stalagmite Y99 studied here is referred to as section I. Two ^{230}Th ages measured at the top and base of stalagmite P3 (see Table 1 and Fig. 2) indicate that it grew within the time period of about 10 to 1.3 ka BP. A marked change in colour (arrow in Fig. 2) close to the top of P3 indicates a growth hiatus. The existing ages do not allow drawing conclusions on the timing of the growth hiatus, and the chronology of P3 is thus only poorly constrained.

2.3 Stable isotope analyses

Oxygen isotopes for stalagmites Y99 and P3 were analyzed on a Finnigan Delta V Advantage mass spectrometer equipped with an automated carbonate preparation system (Gas Bench-II, see Fleitmann et al. (2011) for analytical details). $\delta^{18}O_{calcite}$ measurements of stalagmite D1 were performed on a Delta-plusXL mass spectrometer and are published in Fleitmann et al. (2007). $\delta^{18}O_{calcite}$ values are presented as parts per mil (‰) relative to the Vienna PeeDee Belemnite (VPDB) standard.

2.4 Water yield measurements

Inclusion water was extracted from 30 samples of stalagmite D1, 13 samples of stalagmite P3, and 5 samples of stalagmite Y99. The extracted water amounts, i.e. the water yields (defined as the amounts of water extracted per unit mass of stalagmite rock), as well as total water contents (defined as the total amount of water per unit mass of stalagmite rock) are given as mass of water per unit mass of stalagmite rock in Table 2 and throughout the paper. Prior to water extraction, each sample was first crushed to a grain size of about 350 µm. Crushed samples (approximately 5 g for D1 and P3, ≤1 g for Y99 samples) were then loaded into a high vacuum water and noble gas extraction system (Scheidegger et al., 2010, 2011). Water was extracted from the grain separates by heating. The extracted amounts of water were then determined by concentrating the water into a known volume and measuring the water vapour pressure

CPD
8, 2893–2920, 2012

manometrically following the experimental procedure described by Scheidegger et al. (2010). At temperatures above approximately 600 °C, water extraction from the samples is quantitative, as at these temperatures calcite begins to disintegrate into CaO and CO_2 (e.g. Faust, 1950; Yonge, 1982). The generated CO_2 however would significantly disturb the water vapour pressure measurements (see also Sect. 2.5). Therefore, the grain separates were heated for 1 h to only 320 °C (D1 and P3 samples), and 400 °C (Y99 samples), respectively. The resulting water yields are considerably lower than the total water contents of the samples. The water yield is mainly a function of the extraction temperature and duration, but also of the texture of a given stalagmite sample. Therefore, a direct comparison of water yields is only meaningful for samples taken from the same stalagmite, and only if extraction was performed under the same experimental conditions for all samples.

2.5 Additional water extraction experiments

In order to further study the relationship between water yield and the total water content of the samples, additional water extraction experiments were performed. Small blocks (1–5 g) were cut from stalagmites D1 and P3 close to the positions of samples used for water yield determinations to enable a direct comparison of the respective extracted water amounts. The blocks were broken into few pieces and loaded into a vacuum crusher described by Scheidegger et al. (2010). In a first step, each sample was crushed to a very fine powder (50–80 wt% of the powder had a grain size of <85 µm), and the water amount released during crushing was determined. In a second step, this powder was heated to 480 °C for 1 h to extract as much water as possible at conditions that still allowed determination of an accurate water vapour pressure. The cumulative water yields extracted during crushing and subsequent heating to 480 °C are referred to as "water yield crushing + heating 480 °C" in Table 2 and Fig. 3. For both stalagmites, a correlation was observed between the water yields obtained from extraction at 320 °C and the combined crushing/heating procedure (Fig. 3). The latter water amounts are systematically higher by about a factor of 10 compared to the

CPD
8, 2893–2920, 2012

former ones. Interestingly, the fractions of water released during crushing alone (i.e., prior to heating the powder to 480 °C) are significantly different for D1 and P3 samples. In the case of P3, about 70 % of the extracted water was released by crushing, followed by another 30 % by heating of the crushed sample. For D1 samples about 40 % of the water was released during crushing and 60 % by subsequent heating.

Subsequent to the 480 °C heating step, two samples of D1 were heated to 650 °C for 1 h, a temperature at which calcite begins to decompose (Faust, 1950; Yonge, 1982) and water extraction is quantitative (Yonge, 1982). In both cases, the extensive heating caused a gas pressure that, if generated by water vapour, would have been approximately equivalent to another 40 % of water released from the samples. However, under these conditions the gas pressure is largely controlled by the generation of CO_2 from calcite (Scheidegger et al., 2010), and only a minor fraction of it is actually related to water vapour. We therefore conclude that the water yields from the combined crushing and heating to 480 °C are close to the total water contents of the samples.

The experiments show that water extraction from stalagmite samples occurs in a highly systematic manner. The correlation shown in Fig. 3 illustrates that the water yield is a quantity intrinsic to each stalagmite sample and can be used as a proxy for its total water content.

2.6 Microscopy

Optical inspection of stalagmite thin sections was performed using a Zeiss Axioplan 2 optical microscope equipped with a DeltaPix camera and software. Thin sections were prepared from parts of stalagmites D1 (thin sections D1-A, -B, -C) and P3 (thin sections P3-A, -B) characterized by higher and lower water yields, respectively, in order to compare measured water yields with volume fractions of inclusions estimated from optical inspection (see Fig. 2 for locations of thin section in stalagmites D1 and P3). The thin sections showed that inclusions were numerous and heterogeneous in size, shape, and distribution. Thus, neither counting nor a distinction into (originally) water- and gas-filled inclusions was practicable. Therefore, 8–16 microphotographs were taken at suitable

CPD
8, 2893–2920, 2012

magnifications and under transmitted light for each of the thin sections and were transformed into black and white images applying a greyscale threshold (see Figs. 4 and 5). The threshold was selected such that only inclusions at the immediate surface (i.e. open cavities and inclusions located within the uppermost few microns of the sections), and not those from deeper parts of the sections, appeared as black areas in the processed images. For all P3 images the same threshold value was used, for D1 images the threshold values varied slightly due to variable greyscale distributions of the original photographs. Subsequently, the fraction of black pixels was determined for each image, and the results from all images of the same thin section were averaged. The resulting mean values (given with the respective standard errors of the means in the results section) served as an estimate of the volume of fluid inclusions per unit volume of stalagmite rock. We thereby imply that a sample with a high volume fraction of fluid inclusions (i.e., comprising both water- and gas-filled inclusions), is also characterized by a high volume fraction of water-filled inclusions alone and vice versa.

3 Results

3.1 Water yields and oxygen isotopes

Figure 6 shows for D1, P3, and Y99 the correlations of water yields with $\delta^{18}O_{calcite}$ values. For this comparison, the resolutions of both parameters had to be adjusted, because samples for water yield analyses were taken with spatial resolutions of 1 cm, while samples for oxygen isotope measurements were taken at resolutions of about 2 mm (D1), 5 mm (P3), and 1 mm (Y99). Therefore, $\delta^{18}O_{calcite}$ values were averaged such that each water yield data point was compared with the mean of the spatially closest 5 (D1), 3 (P3), and 9 (Y99) $\delta^{18}O_{calcite}$ values. A correlation between the parameters water yield and $\delta^{18}O_{calcite}$ is obvious in all three stalagmites and significant on the 5 % level or better (Fig. 6). For all three stalagmites low water yields correspond to low $\delta^{18}O_{calcite}$ values and vice versa.

CPD
8, 2893–2920, 2012

The observed correlation between water yield and oxygen isotopic composition was further assessed by applying parametric Sequential t-test Analyses of Regime Shifts (STARS, Rodionov, 2004; Rodionov and Overland, 2005) to determine regime shift points in the stalagmites' $\delta^{18}O_{calcite}$ records. Thereby, the targeted significance level p was predefined to 0.05 and for the window length L we used 10, 20, and 30 data points, respectively. The most prominent regime shift point for each $\delta^{18}O_{calcite}$ record is shown as a dashed red line in Fig. 7. Subsequently, the water yield and $\delta^{18}O_{calcite}$ values on both sides of the respective major shift points were compared with each other by means of the Student's t-test. Mean values with standard errors of the means for all oxygen and water yield data prior and after the respective major regime shift points are given in Fig. 7 and are additionally visualized as grey areas in the plots.

3.1.1 Stalagmite D1 (Fig. 7a)

The D1 $\delta^{18}O_{calcite}$ ranges around values of about −3 ‰ between 4.35 and 1.3 ka BP, followed by an overall decrease of the $\delta^{18}O_{calcite}$ values between 1 ka BP to the present. STARS determines the major regime shift point in the D1 oxygen isotope record at 1.25 ka BP, which corresponds to a pronounced negative excursion with $\delta^{18}O_{calcite}$ values as low as −5.3 ‰. Note that each of the different window lengths applied resulted in the same major regime shift point. Application of the Student's t-test shows that the D1 $\delta^{18}O_{calcite}$ values prior to and after the major regime shift point are significantly different from each other at the 1 ‰ level. Accordingly, also the water yields on both sides of the major regime shift point (as defined via the $\delta^{18}O_{calcite}$ data) are different from each other at the 1 ‰ level.

3.1.2 Stalagmite P3 (Fig. 7b)

The P3 $\delta^{18}O_{calcite}$ values range around −2 ‰ between 53 and 7 cm from the top of the stalagmite. In contrast, the character of the $\delta^{18}O_{calcite}$ record of the uppermost few centimeters of P3 is clearly different showing a distinctly larger variability of $\delta^{18}O_{calcite}$

CPD
8, 2893–2920, 2012

values over small distances with individual values of up to +0.5 ‰. STARS detects the major regime shift point at 6 cm distance from the top of the stalagmite, again using window lengths L of 10, 20, and 30 data points, respectively. Indeed, the P3 $\delta^{18}O_{calcite}$ values on both sides of the regime shift point are significantly different from each other at the 1 % level. Also the water yield values on both sides of the regime shift point at 6 cm distance from the top are different from each other at the 5 % significance level.

3.1.3 Stalagmite Y99 (Fig. 7c)

The Y99 $\delta^{18}O_{calcite}$ values range around −11 ‰ between 131 and 121 ka BP. Like P3, also Y99 shows in its youngest part (121–119 ka BP) a distinctly larger variability of $\delta^{18}O_{calcite}$ values over small distances with individual values of up to −6 ‰. For this $\delta^{18}O_{calcite}$ record STARS detects the major regime shift point at 120.6 ka BP. The $\delta^{18}O_{calcite}$ values on both sides of this shift point location are significantly different from each other at the sub-permil level. Also the water yields prior and after the major regime shift point are different from each other at a significance level of 1 %.

As shown in Fig. 7, for all three stalagmites low mean water yields correlate with low mean $\delta^{18}O_{calcite}$ and vice versa, corroborating the results from the direct comparison of both parameters described above and shown in Fig. 6.

3.2 Relationship between water yield and the occurrence of microscopically detectable fluid inclusions

Image-processed microphotographs of thin sections were used to optically estimate volume fractions of fluid inclusions from parts of stalagmites D1 and P3 characterized by high and low water yields, respectively.

Thin sections D1-A and D1-B were prepared from the upper part of stalagmite D1 characterized by low water yields. The volume fractions of fluid inclusions for D1-A and D1-B are (2.6 ± 0.3) % and (2.7 ± 0.3) %, respectively. Thin section D1-C was prepared

CPD
8, 2893–2920, 2012

from the lower part of the stalagmite characterized by high water yields, and also shows a higher volume fraction of fluid inclusions of (3.7 ± 0.3) % compared to D1-A and -B.

For thin section P3-A, prepared from the top of the stalagmite with overall high water yields, the volume fraction of fluid inclusions is (2.4 ± 0.4) %. Thin section P3-B, prepared from a lower part of the stalagmite characterized by low water yields, also shows a slightly lower volume fraction of fluid inclusions of (2.0 ± 0.8) %.

The results from optical inspection of thin sections support those from our actual water yield measurements. For both stalagmites, those parts characterized by high water yields also show large volume fractions of fluid inclusions and vice versa. Nonetheless, we emphasize that especially the selection of appropriate threshold values to distinguish fluid inclusions (both air- and water-filled) from other features (e.g. surface roughness) of the thin sections is to a certain degree subject to the examiner's personal judgement, which might bias the respective results. Thus, in order to infer for a given set of stalagmite samples a reliable record of water contents, extraction of inclusion water under uniform experimental conditions is certainly preferable to the more subjective tool of microscopic inspection of thin sections.

4 Water yield, oxygen isotopes, and drip water supply

Numerous oxygen isotope studies on stalagmites from Yemen and Oman have shown that $\delta^{18}O_{calcite}$ records reflect precipitation rates in the area with decreasing $\delta^{18}O_{calcite}$ values indicating increasing precipitation rates and vice versa (e.g. Burns et al., 1998, 2001; Fleitmann et al., 2003a, b, 2004, 2007, 2011).

The oxygen isotope record of stalagmite D1 is characterized by fairly constant precipitation on Socotra Island between 4.3 to 1.2 ka BP. From 1.2 ka BP to the present, $\delta^{18}O_{calcite}$ values decrease considerably, which indicates an increase in precipitation rates (see also, Fleitmann et al., 2007).

Also the $\delta^{18}O_{calcite}$ pattern of stalagmite P3 implies fairly constant precipitation over large parts of the record. The uppermost few centimeters of P3 are characterized by

CPD
8, 2893–2920, 2012

rapidly changing $\delta^{18}O_{calcite}$ values over short distances including two prominent excursions to high $\delta^{18}O_{calcite}$ values at around 4.5 cm and 0 cm from the top of the stalagmite. The peak at 4.5 cm correlates with a distinctive dark layer indicative of a growth hiatus (see Figs. 2 and 7b). The second increase of $\delta^{18}O_{calcite}$ at 0 cm correlates with the final termination of stalagmite growth. A corresponding carbon isotope record of stalagmite P3 (not shown) shows two excursions towards high $\delta^{13}C_{calcite}$ values synchronous with the positive $\delta^{18}O_{calcite}$ peaks. We conclude that the excursions to higher, i.e. heavier isotopic compositions for both oxygen and carbon are the result of reduced drip water availability leading to higher rates of CO_2 degassing from the water film on top of stalagmite P3. This process is known to cause simultaneous enrichment of ^{13}C and ^{18}O in the precipitating calcite (e.g. Baker et al., 1997; Hendy, 1971).

The interpretation of the section of Y99 studied here is similar to that of P3. Between 131 and 121 ka BP, high precipitation rates lead to the lowest mean $\delta^{18}O_{calcite}$ values found in the stalagmite (cf., Fleitmann et al., 2011). The time span between 121 and 119 ka BP is characterized by strongly variable $\delta^{18}O_{calcite}$ values including prominent excursions to higher, i.e. heavier $\delta^{18}O_{calcite}$ values similar to those found in P3. This implies an overall reduction of drip water supply between 121 and 119 ka BP, ultimately followed by the termination of growth of stalagmite Y99.

The interpretation of $\delta^{18}O_{calcite}$ in terms of drip water supply allows establishing a link between water yields of the studied stalagmites and drip rates. $\delta^{18}O_{calcite}$ in D1 indicates a period of constant precipitation, implying a constant drip water supply, between 4.3 and 1.2 ka BP. During the last 1 ka BP precipitation, and therefore also the drip rates for D1 increase. During the same time interval D1 shows reduced water yields in the respective stalagmite samples. Therefore, we infer that the fraction of water-filled inclusions (governing the water yield of a given sample) in the stalagmite is reduced during times of higher drip water supply. The P3 and Y99 $\delta^{18}O_{calcite}$ data both indicate phases of fairly constant precipitation and therefore constant drip rates. These are followed by periods of lower precipitation and thus lower drip rates recorded in the uppermost few

CPD
8, 2893–2920, 2012

cm of the two stalagmites, respectively. For both stalagmites, these uppermost parts are also characterized by the highest water yields. Consequently, we conclude that a reduction of drip water supply increases the fraction of water-filled inclusions in the growing stalagmite.

This conclusion might at first sight be "counterintuitive". However, our observations are supported by several studies on stalagmite growth and formation of stalagmite fluid inclusions (e.g. Fairchild et al., 2008; Frisia et al., 2000; Genty and Quinif, 1996; Yonge, 1982). All studies agree that a high supply of drip water, being usually characterized by low calcium ion supersaturation (e.g. Sherwin, 2011), supports a slow and constant growth of calcite crystals, which results in a low density of crystal defects. Such "ideal" crystal growth conditions lead to a low porosity and therefore a low fraction of fluid inclusions in the calcite precipitate. Low drip rates (with high calcium ion supersaturation of the water) lead to a more effective degassing of CO_2 from the drip water, which in turn causes faster carbonate precipitation. In addition, low drip rates can cause periodic exposure of the growing crystals to the cave air. Both effects result in a "non-ideal" crystal growth and a higher porosity, and therefore a larger fraction of fluid inclusions in the calcite fabric (Fairchild et al., 2008; Frisia et al., 2000; Genty and Quinif, 1996).

5 Conclusions

We present water yield measurements, serving as proxy measures of the total water content of stalagmite samples, together with oxygen isotope records for two Holocene stalagmites from Socotra Island, Yemen, and one Eemian stalagmite from southern continental Yemen. Water yield measurements are qualitatively supported by the volume fractions of fluid inclusions in the stalagmites, estimated from optical inspection of stalagmite thin sections. Water yields vary systematically with changes in the oxygen isotopic compositions of a given stalagmite. Thereby, isotopically light oxygen is accompanied by low water yields and vice versa. Based on the paleoclimatic interpretation of the stalagmites' $\delta^{18}O_{calcite}$ records in terms of drip water supply, we infer

CPD
8, 2893–2920, 2012

that stalagmite samples with low water yields formed during times of increased drip water supply, allowing undisturbed calcite growth and thus leading to inclusion-poor stalagmite rock and vice versa. We therefore propose that for stalagmites from tropical or subtropical areas, water yield records allow direct conclusions on changes in drip rates which in turn can be used to track changes in the rates of precipitation. Further research will have to show whether or not this new paleoclimate proxy can also be applied to stalagmites grown under different climatic conditions.

Acknowledgement. The authors would like to thank U. Menet and H. Baur for their assistance in the noble gas laboratory at ETH Zurich. We also thank Y. Krüger (University of Berne) for his valuable input concerning the formation of fluid inclusions. We are grateful to M. G. Fellin for her help with and frequent and unbuerocratic access to various optical microscopes at ETH Zurich. Inspiring and helpful discussions with all members of the Environmental Isotope Group at Eawag are greatly acknowledged, as are comments on an earlier version of the manuscript by anonymous reviewers. This study was carried out in the framework of the Sinergia project "STALCLIM" funded by the Swiss National Science Foundation (grant no. CRSI22-132646/1 to D. Fleitmann and co-PI's).

References

Baker, A., Ito, E., Smart, P. L., and McEwan, R. F.: Elevated and variable values of ^{13}C in speleothems in a British cave system, Chem. Geol., 136, 263–270, 1997.

Burns, S. J., Matter, A., Frank, N., and Mangini, A.: Speleothem-based paleoclimate record from Northern Oman, Geology, 26, 499–502, 1998.

Burns, S. J., Fleitmann, D., Matter, A., Neff, U., and Mangini, A.: Speleothem evidence from Oman for continental pluvial events during interglacial periods, Geology, 29, 623–626, 2001.

Cheng, H., Edwards, R. L., Broecker, W. S., Denton, G. H., Kong, X., Wang, Y., Zhang, R., and Wang, X.: Ice age terminations, Science, 326, 248–252, 2009.

Clemens, C. C., Prell, W. L., and Sun, Y.: Orbital-scale timing and mechanisms driving Late Pleistocene Indo-Asian summer monsoons: reinterpreting cave speleothem $\delta^{18}O$, Paleoceanography, 25, PA4207, doi:10.1029/2010PA001926, 2010.

CPD
8, 2893–2920, 2012

Cosford, J., Quing, H., Mattey, D., Eglington, B., and Zhang, M.: Climatic and local effects on stalagmite δ^{13}C values at Lianhua Cave, China, Palaeogeogr. Palaeocl., 280, 235–244, 2009.

Dong, J., Wang, Y., Cheng, H., Hardt, B., Edwards, R. L., Kong, X., Wu, J., Chen, S., Liu, D., Jiang, X., and Zhao, K.: A high-resolution stalagmite record of the Holocene East Asian monsoon from Mt Shennongjia, Central China, Holocene, 20, 257–264, 2010.

Dorale, J. A., Edwards, R. L., Ito, E., and Gonzales, L. A.: Climate and vegetation history of the midcontinent from 75 to 25 ka: a speleothem record from Crevice Cave, Missouri, USA, Science, 282, 1871–1874, 1998.

Fairchild, I. J., Frisia, S., Borsato, A., and Tooth, A. F.: Speleothems, in: Geochemical Sediments and Landscapes, edited by: Nash, D. J. and McLaren, S. J., Blackwell Publishing Ltd., Oxford, UK, 200–245, 2008.

Faust, G. T.: Thermal analysis studies on carbonates: 1. aragonite and calcite, Am. Mineral., 35, 207–224, 1950.

Fleitmann, D., Burns, S. J., Mudelsee, M., Neff, U., Kramers, J., Mangini, A., and Matter, A.: Holocene forcing on the Indian monsoon recorded in a stalagmite from Southern Oman, Science, 300, 1737–1739, 2003a.

Fleitmann, D., Burns, S. J., Neff, U., Mangini, A., and Matter, A.: Changing moisture sources over the last 330 000 years in Northern Oman from fluid-inclusions evidence in speleothems, Quarternary Res., 60, 223–232, 2003b.

Fleitmann, D., Burns, S. J., Neff, U., Mudelsee, M., Mangini, A., and Matter, A.: Paleoclimatic interpretation of high-resolution oxygen isotope profiles derived from annually laminated speleothems from Southern Oman, Quart. Sci. Rev., 23, 935–945, 2004.

Fleitmann, D., Burns, S. J., Mangini, A., Mudelsee, M., Kramers, J., Villa, I., Neff, U., Al-Subbary, A. A., Buettner, A., Hippler, D., and Matter, A.: Holocene ITCZ and Indian monsoon dynamics recorded in stalagmites from Oman and Yemen (Socotra), Quart. Sci. Rev., 26, 170–188, 2007.

Fleitmann, D., Cheng, H., Badertscher, S., Edwards, R. L., Mudelsee, M., Göktürk, O. M. A. F., Pickering, R., Raible, C. C., Matter, A., Kramers, J., and Tüysüz, O.: Timing and climatic impact of Greenland interstadials recorded in stalagmites from Northern Turkey, Geophys. Res. Lett., 36, L19707, doi:10.1029/2009GL040050, 2009.

CPD
8, 2893–2920, 2012

Fleitmann, D., Burns, S. J., Pekala, M., Mangini, A., Al-Subbary, A. A., Al-Aowah, M., Kramers, J., and Matter, A.: Holocene and Pleistocene pluvial periods in Yemen, Southern Arabia, Quart. Sci. Rev., 30, 783–787, 2011.

Frisia, S., Borsato, A., Fairchild, I. J., and McDermott, F.: Calcite fabrics, growth mechanisms, and environments of formation in speleothems from the Italian Alps and Southwestern Ireland, J. Sediment. Res., 70, 1183–1196, 2000.

Genty, D. and Quinif, Y.: Annually laminated sequences in the internal structure of some Belgian stalagmites – importance for paleoclimatology, J. Sediment. Res., 66, 275–288, 1996.

Griffith, M. L., Drysdale, R. N., Vonhof, H. B., Gagan, M. K., Zhao, J., Ayliffe, L. K., Hantoro, W. S., Hellstorm, J. C., Cartwright, I., Frisia, S., and Suwargadi, W.: Younger Dryas – Holocene temperature and rainfall history of southern Indonesia from $\delta^{18}O$ in speleothem calcite and fluid inclusions, Earth Planet. Sci. Lett., 295, 30–36, 2010.

Harmon, R. S., Schwarcz, H. P., and O'Neil, J. R.: D/H ratios in speleothem fluid inclusions: a guide to variations in the isotopic composition of meteoric precipitation, Earth Planet. Sci. Lett., 42, 254–266, 1979.

Henderson, G. M.: Caving in to new chronologies, Science, 313, 620–622, 2006.

Hendy, C. H.: The isotopic geochemistry of speleothems – I. The calculation of the effects of different modes of formation on the isotopic composition of speleothems and their applicability as paleoclimatic indicators, Geochim. Cosmochim. Ac., 35, 801–824, 1971.

Kluge, T., Marx, T., Scholz, D., Niggemann, S., Mangini, A., and Aeschbach-Hertig, W.: A new tool for paleoclimate reconstruction: noble gas temperatures from fluid inclusions in speleothems, Earth Planet. Sci. Lett., 269, 408–415, 2008.

LeGrande, A. N. and Schmidt, G. A.: Sources of Holocene variability of oxygen isotopes in paleoclimate archives, Clim. Past, 5, 441–455, doi:10.5194/cp-5-441-2009, 2009.

Liu, D., Wang, Y., Cheng, H., Edwards, R. L., Kong, X., Wang, X., Hardt, B., Wu, J., Chen, S., Jiang, X., He, Y., Dong, J., and Zhao, K.: Sub-millennial variability of Asian monsoon intensity during the early MIS 3 and its analogue to the ice age terminations, Quarternary Sci. Rev., 29, 1107–1115, 2010.

McDermott, F., Schwarcz, H. P., and Rowe, P. J.: Isotopes in Speleothems, in: Isotopes in paleoenvironmental research, edited by: M. J. Leng, Springer, Dordrecht, The Netherlands, 307, 185–225, 2006.

McGarry, S., Bar-Matthews, M., Matthews, A., Vaks, A., Schilmann, B., and Ayalon, A.: Constraints on hydrological and paleotemperature variations in the Eastern Mediterranean region

CPD
8, 2893–2920, 2012

in the last 140 ka given by the δD values of speleothem fluid inclusions, Quaternary Sci. Rev., 23, 919–934, 2004.
Rodionov, S. N.: A sequential algorithm for testing climate regime shifts, Geophys. Res. Lett., 31, L09204, doi:10.1029/2004GL019448, 2004.
Rodionov, S. N. and Overland, J. E.: Application of a sequential regime shift detection method to the Bering Sea ecosystem, J. Mar. Sc., 62, 328–332, 2005.
Scheidegger, Y. M., Baur, H., Brennwald, M. S., Fleitmann, D., Wieler, R., and Kipfer, R.: Accurate analysis of noble gas concentrations in small water samples and its application to fluid inclusions in stalagmites, Chem. Geol., 272, 31–39, 2010.
Scheidegger, Y. M., Brennwald, M. S., Fleitmann, D., Jeannin, P.-Y., Wieler, R., and Kipfer, R.: Determination of Holocene cave temperatures from Kr and Xe concentrations in stalagmite fluid inclusions, Chem. Geol., 288, 61–66, 2011.
Scholte, P. and De Geest, P.: The climate of Socotra Island (Yemen): a first-time assessment of the timing of the monsoon wind reversal and its influence on precipitation and vegetation patterns, J. Arid Environ., 74, 1507–1515, 2010.
Schwarcz, H. P. and Harmon, R. S.: Stable isotope studies of fluid inclusions in speleothems and their paleoclimatic significance, Geochim. Cosmochim. Ac., 40, 657–665, 1976.
Shakun, J. D., Burns, S. J., Fleitmann, D., Kramers, J., Matter, A., and Al-Subary, A.: A high-resolution, absolute-dated deglacial speleothem record of Indian Ocean climate from Socotra Island, Yemen, Earth Planet. Sci. Lett., 259, 441–456, 2007.
Sherwin, C. M.: Cave air and hydrological controls on prior calcite precipitation and stalagmite growth rates: implications for paleoclimate reconstructions using speleothems, Geochim. Cosmochim. Ac., 75, 3915–3929, 2011.
Vaks, A., Bar-Matthews, M., Matthews, A., Ayalon, A., and Frumkin, A.: Middle-Late Quaternary paleoclimate of northern margins of the Saharan-Arabian desert: reconstruction from speleothems of Negev Desert, Israel, Quarternary Sci. Rev., 29, 2647–2662, 2010.
Wang, Y., Cheng, H., Edwards, R. L., Kong, X., Shao, X., Chen, S., Wu, J., Jiang, X., Wang, X., and An, Z.: Millennial- and orbital-scale changes in the East Asian monsoon over the past 224 000 years, Nature, 451, 1090–1093, 2008.
Yonge, C. J.: Stable isotope studies from the water extracted from speleothems, PhD Thesis, McMaster University, Hamilton, 298 pp., 1982.
Zhang, R., Schwarcz, H. P., Ford, D. C., Serefiddin Schroeder, F., and Beddows, P. A.: An absolute paleotemperature record from 10 to 6 ka inferred from fluid inclusion D/H ratios of

CPD
8, 2893–2920, 2012

a stalagmite from Vancouver Island, British Columbia, Canada, Geochim. Cosmochim. Ac., 72, 1014–1026, 2008.

Zhao, K., Wang, Y., Edwards, R. L., Cheng, H., and Liu, D.: High-resolution stalagmite $\delta^{18}O$ records of Asian monsoon changes in Central and Southern China spanning the MIS 3/2 transition, Earth Planet. Sci. Lett., 298, 191–198, 2010.

CPD

8, 2893–2920, 2012

Table 1. Results of ^{230}Th-dating of stalagmite P3 (see Fleitmann et al. (2007) for details on the analytical techniques).

Sample	Distance from top (cm)	c(Th) (ppb)	c(U) (ppb)	^{234}U/^{238}U	^{230}Th/^{232}Th	^{230}Th/^{234}U	Age (ka BP)
P3-a	0.5	0.496 ± 0.007	330.7 ± 0.9	1.2408 ± 0.0033	31 ± 2	0.0123 ± 0.0007	1.34 ± 0.09
P3-b	75	0.176 ± 0.001	376 ± 1	1.2778 ± 0.0039	760 ± 11	0.0920 ± 0.0011	10.5 ± 0.2

CPD
8, 2893–2920, 2012

Table 2. Water in stalagmites D1 and P3.

Sample	Age (ka BP)	Water yield 320 °C (10^{-4} g g^{-1})	Water yield crushing+heating 480 °C (10^{-4} g g^{-1})	Sample	Distance from top (cm)	Water yield 320 °C (10^{-4} g g^{-1})	Water yield crushing+heating 480 °C (10^{-4} g g^{-1})
D1-1	0.04	1.96 ± 0.02		P3-1	0.5	3.33 ± 0.04	
D1-2	0.07	2.58 ± 0.03		P3-2	0.5	3.30 ± 0.04	
D1-3	0.19	1.77 ± 0.02		P3-3	1	2.92 ± 0.04	
D1-4	0.30	2.22 ± 0.03		P3-4	2	1.80 ± 0.02	18.3 ± 0.3
D1-5	0.37	2.53 ± 0.03	26.4 ± 0.4	P3-5	3	3.55 ± 0.04	
D1-6	0.74	3.31 ± 0.04		P3-6	7.3	2.87 ± 0.03	36.2 ± 0.3
D1-7	1.60	3.02 ± 0.04		P3-7	13	2.29 ± 0.03	13.1 ± 0.6
D1-8	1.75	4.96 ± 0.08		P3-8	20	2.13 ± 0.03	
D1-9	1.80	3.50 ± 0.04		P3-9	27	2.12 ± 0.03	23.6 ± 0.2
D1-10	1.85	4.73 ± 0.06		P3-10	41	1.58 ± 0.02	
D1-11	1.89	5.85 ± 0.07		P3-11	45	0.86 ± 0.01	7.3 ± 0.2
D1-12	1.90	5.30 ± 0.06		P3-12	51	1.72 ± 0.02	
D1-13	1.95	3.76 ± 0.04		P3-13	69	2.87 ± 0.03	28.1 ± 0.2
D1-14	2.00	4.70 ± 0.06					
D1-15	2.05	3.07 ± 0.04					
D1-16	2.10	2.98 ± 0.04					
D1-17	2.15	3.43 ± 0.04					
D1-18	2.20	3.70 ± 0.04	32.4 ± 0.4				
D1-19	2.37	6.00 ± 0.07					
D1-20	2.45	4.45 ± 0.05					
D1-21	3.13	2.07 ± 0.02					
D1-22	3.14	3.75 ± 0.05					
D1-23	3.19	5.20 ± 0.06					
D1-24	3.49	3.74 ± 0.04	47.4 ± 0.6				
D1-25	3.72	3.88 ± 0.05					
D1-26	3.80	3.60 ± 0.04					
D1-27	4.28	4.86 ± 0.06					
D1-28	4.32	4.30 ± 0.05	43.0 ± 0.4				
D1-29	4.53	4.55 ± 0.05					
D1-30	4.56	4.04 ± 0.05					

Sample	Age (ka BP)	Water yield 400 °C (10^{-4} g g^{-1})
Y99-1	119.7	21.3 ± 0.6
Y99-2	119.7	21.2 ± 0.6
Y99-3	124.2	10.3 ± 0.2
Y99-4	126.5	5.98 ± 0.08
Y99-5	129.2	7.9 ± 0.1

D1, P3, and Y99 water yields extracted from grain separates (mean grain diameter 350 µm) at different temperatures. For selected samples of D1 and P3 also the water yield resulting from combined vacuum crushing and subsequent heating of the powder to 480 °C ("water yield crushing + heating 480 °C") is given. Uncertainties of water yield measurements take into account the precision of the manometer and the uncertainty introduced by a residual hydrogen pressure (for details, see Scheidegger et al., 2010, 2011). ^{230}Th age uncertainties are <3 %. For detailed information on the age uncertainties of D1 and Y99 see Fleitmann et al. (2007) and Fleitmann et al. (2011), respectively.

CPD
8, 2893–2920, 2012

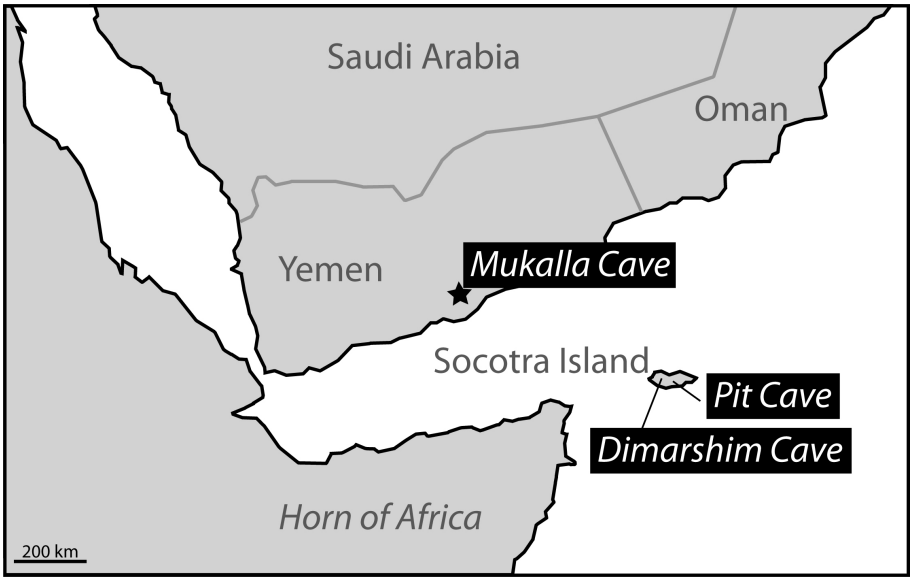

Fig. 1. Overview map showing Yemen with Socotra Island and the locations of Mukalla Cave, Dimarshim Cave, and Pit Cave.

CPD
8, 2893–2920, 2012

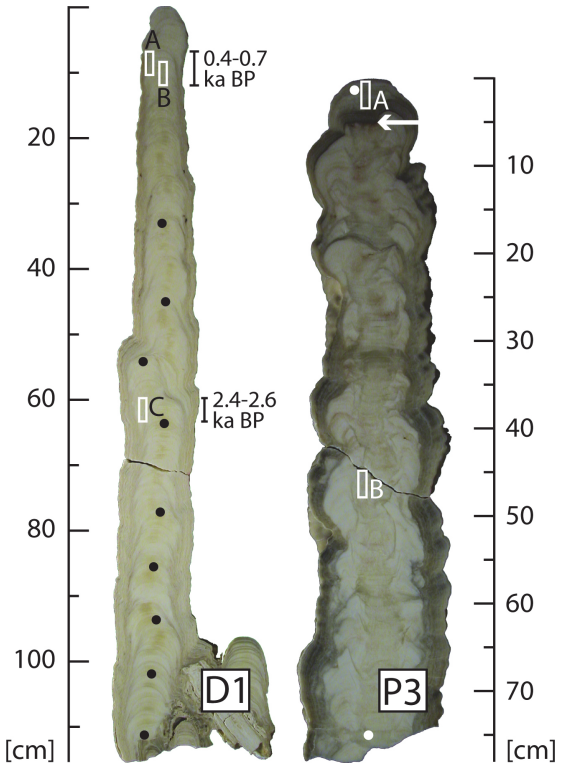

Fig. 2. Photographs of polished sections of stalagmites D1 and P3 cut parallel to their growth axes including locations for ^{230}Th dating (black dots for D1, white dots for P3). The arrow points to a potential growth hiatus in stalagmite P3. White squares indicate areas from which thin sections for stalagmite D1 (D1-A, -B, -C) and P3 (P3-A, -B) were prepared. For D1 sections also the approximate covered time intervals are given. Photographs for Y99 with locations for dating are presented in Fleitmann et al. (2011).

CPD
8, 2893–2920, 2012

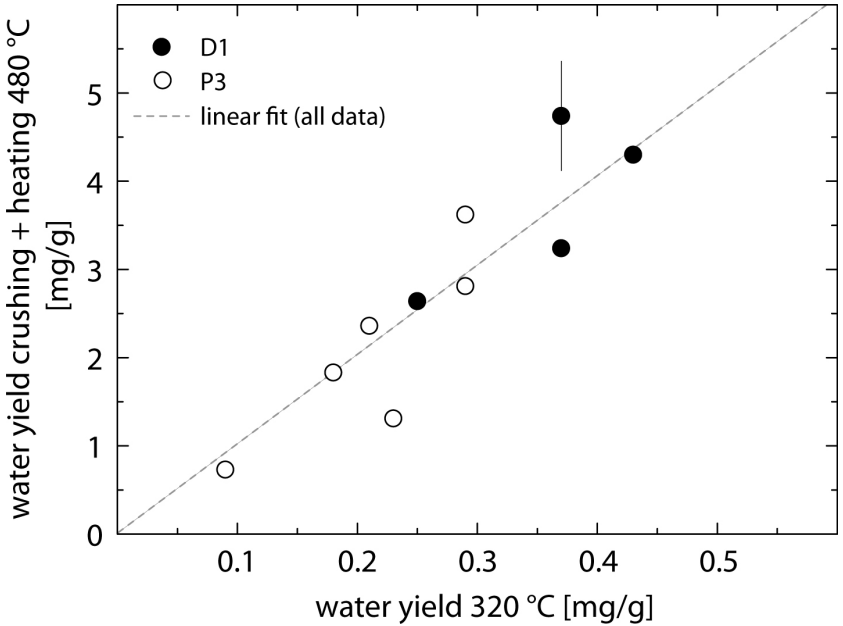

Fig. 3. Comparison of water yields resulting from heating to 320 °C and from crushing and subsequent heating to 480 °C of selected samples of stalagmites P3 and D1. Both quantities are linearly correlated (coefficient of determination r^2 = 0.97). Uncertainties of water yield determinations are, with one exception, smaller than the symbol sizes.

CPD
8, 2893–2920, 2012

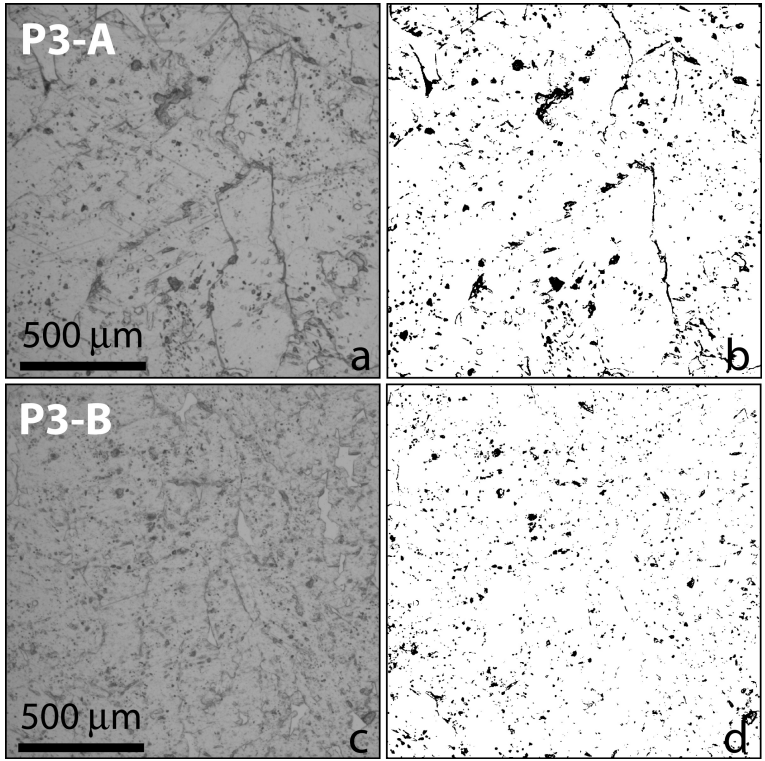

Fig. 4. Examples of microphotographs of stalagmite thin sections P3-A **(a)** and P3-B **(c)** characterized by higher and lower water yields, respectively. Also shown are their respective processed black and white images **(b, d)**, in which inclusions at the thin sections' surface are visible as black pixels. Images **(b)** (P3-A) and **(d)** (P3-B) show 6.8 % and 4.3 % of black pixels, respectively.

CPD
8, 2893–2920, 2012

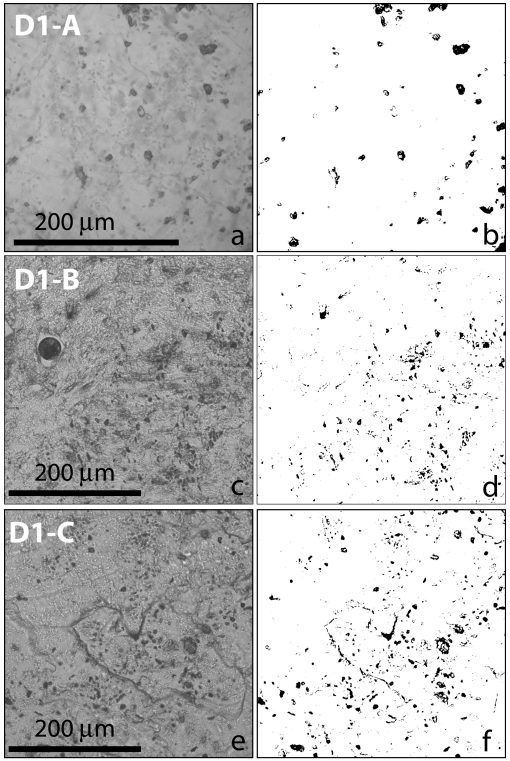

Fig. 5. Examples of microphotographs of stalagmite thin sections D1-A **(a)** and D1-B **(c)**, both characterized by lower water yields, and thin section D1-C **(e)** from an area characterized by higher water yields. Also shown are the respective processed black and white images **(b, d, f)**. The large dark circle in photograph D1-B **(c)** is an artefact from thin section production and was not taken into account for black pixel counting. Images **(b)** (D1-A) and **(d)** (D1-B) show lower percentages of black pixels (2.3 % and 2.7 %, respectively) than image **(f)** (D1-C, 4.8 %).

CPD
8, 2893–2920, 2012

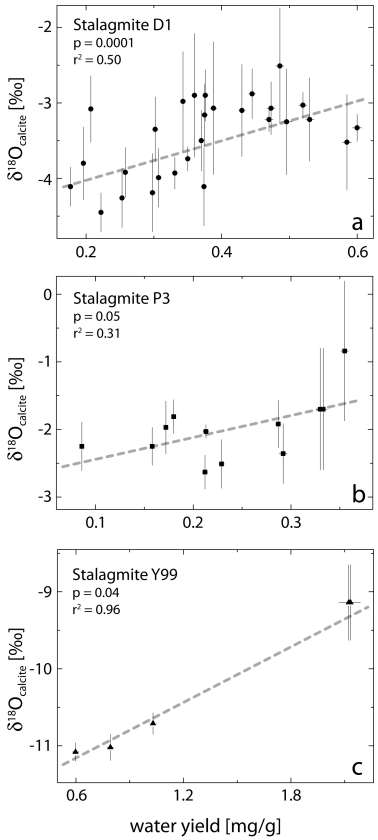

Fig. 6. Correlation between water yield and $\delta^{18}O_{calcite}$ for stalagmites D1 **(a)**, P3 **(b)**, and Y99 **(c)**. Water was extracted at 320 °C for D1 and P3 samples, and at 400 °C for Y99 samples. Error bars of $\delta^{18}O_{calcite}$ values represent standard deviations of mean values.

CPD
8, 2893–2920, 2012

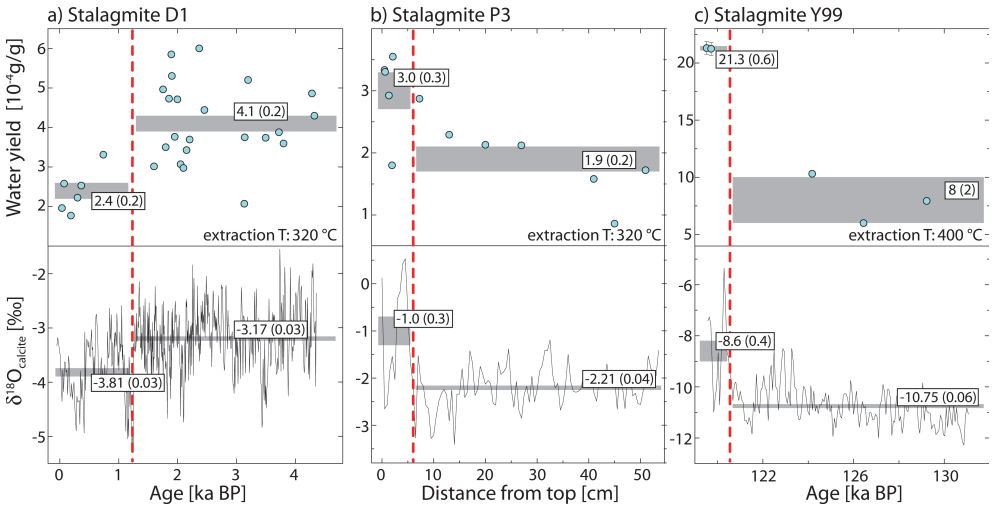

Fig. 7. Water yield and oxygen isotopic compositions of stalagmite D1 **(a)**, P3 **(b)**, and Y99 **(c)** plotted as functions of sample age (D1, Y99), and distance from top (P3). Dashed red lines refer to the major regime shift points as defined from the $\delta^{18}O_{calcite}$ data using STARS (Rodionov, 2004). Numbers in squares represent mean values with standard errors of the means of the data points on both sides of the major regime shift points, respectively. The means are also visualized as grey squares in the plots, the height of the squares corresponding to the standard errors of the means.

CPD
8, 2893–2920, 2012